Article

C9orf72 suppresses systemic and neural inflammation induced by gut bacteria

https://doi.org/10.1038/s41586-020-2288-7

Received: 17 May 2019

Accepted: 9 April 2020

Published online: 13 May 2020

Check for updates

Aaron Burberry[1,2], Michael F. Wells[1,2], Francesco Limone[1,2,3], Alexander Couto[1,2], Kevin S. Smith[1,2], James Keaney[4], Gaëlle Gillet[4], Nick van Gastel[1,5], Jin-Yuan Wang[1,2], Olli Pietilainen[1,2], Menglu Qian[1,2,6], Pierce Eggan[1,2], Christopher Cantrell[1,2], Joanie Mok[1,2], Irena Kadiu[4], David T. Scadden[1,5] & Kevin Eggan[1,2,6]✉

A hexanucleotide-repeat expansion in *C9ORF72* is the most common genetic variant that contributes to amyotrophic lateral sclerosis and frontotemporal dementia[1,2]. The *C9ORF72* mutation acts through gain- and loss-of-function mechanisms to induce pathways that are implicated in neural degeneration[3–9]. The expansion is transcribed into a long repetitive RNA, which negatively sequesters RNA-binding proteins[5] before its non-canonical translation into neural-toxic dipeptide proteins[3,4]. The failure of RNA polymerase to read through the mutation also reduces the abundance of the endogenous *C9ORF72* gene product, which functions in endolysosomal pathways and suppresses systemic and neural inflammation[6–9]. Notably, the effects of the repeat expansion act with incomplete penetrance in families with a high prevalence of amyotrophic lateral sclerosis or frontotemporal dementia, indicating that either genetic or environmental factors modify the risk of disease for each individual. Identifying disease modifiers is of considerable translational interest, as it could suggest strategies to diminish the risk of developing amyotrophic lateral sclerosis or frontotemporal dementia, or to slow progression. Here we report that an environment with reduced abundance of immune-stimulating bacteria[10,11] protects *C9orf72*-mutant mice from premature mortality and significantly ameliorates their underlying systemic inflammation and autoimmunity. Consistent with *C9orf72* functioning to prevent microbiota from inducing a pathological inflammatory response, we found that reducing the microbial burden in mutant mice with broad spectrum antibiotics—as well as transplanting gut microflora from a protective environment—attenuated inflammatory phenotypes, even after their onset. Our studies provide further evidence that the microbial composition of our gut has an important role in brain health and can interact in surprising ways with well-known genetic risk factors for disorders of the nervous system.

To understand the consequences of the long-term reduction in *C9ORF72* activity found in patients with amyotrophic lateral sclerosis (ALS) or frontotemporal dementia (FTD) who carry the repeat expansion, mice that contain loss-of-function (LOF) mutations in the orthologous gene (*C9orf72*) have previously been studied[6,7,12,13]. It was previously reported[7], and later corroborated, that reduced *C9orf72* function led to age-dependent inflammation, characterized by cytokine storm[7,14], neutrophilia[6,7,14], pseudothrombocytopenia[7], autoimmunity[7,14], splenomegaly[6,7,13,14] and neuroinflammation[6,7]. Informed by these observations and validating their importance, it was subsequently found that patients with ALS or FTD who had mutations in *C9ORF72* were significantly more likely to have been diagnosed with autoimmune disease before their neurological diagnosis[15,16].

However, the long-term survival of *C9orf72* LOF mutant mice varied markedly between reports, despite many groups studying the same allele on a similar genetic background. In some studies, it was found[7,12] that the loss of one (+/−) or both (−/−) alleles of *C9orf72* increased the risk of premature mortality, whereas others[13] noted a reduced survival of *C9orf72*$^{-/-}$ but not *C9orf72*$^{+/-}$ mice—and another group[6] reported no survival differences between control and mutant mice (Extended Data Fig. 1). These findings suggested that the environment in which the mice were reared might be an important modifier of survival when *C9orf72* levels are reduced. To test this hypothesis, we aseptically re-derived *C9orf72*-mutant mice into a new facility at the Broad Institute (hereafter referred to as *C9orf72(Broad)* mice) while continuing our colony at the Harvard Biological Research Infrastructure (BRI)

[1]Harvard Stem Cell Institute, Department of Stem Cell and Regenerative Biology, Harvard University, Cambridge, MA, USA. [2]Stanley Center for Psychiatric Research, Broad Institute of MIT and Harvard, Cambridge, MA, USA. [3]Hubrecht Institute for Developmental Biology and Stem Cell Research, Royal Netherlands Academy of Arts and Sciences, Utrecht, The Netherlands. [4]Neuroscience Therapeutic Area, New Medicines, UCB Biopharma SPRL, Braine-l'Alleud, Belgium. [5]Center for Regenerative Medicine, Massachusetts General Hospital, Boston, MA, USA. [6]Department of Molecular and Cellular Biology, Harvard University, Cambridge, MA, USA. ✉e-mail: Eggan@mcb.harvard.edu

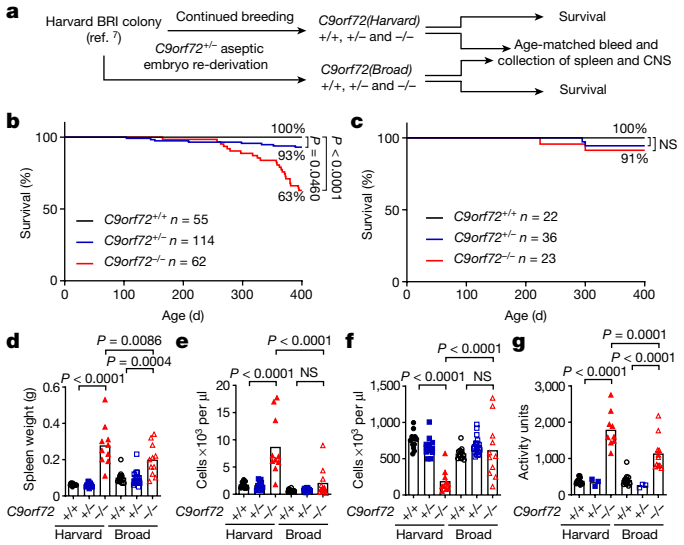

Fig. 1 | Environment governs survival, inflammation and autoimmunity in *C9orf72* LOF mice. a, Aseptic embryo transfer of *C9orf72* neo-deleted allele from Harvard BRI to the Broad Institute. Male and female mice were aged for survival or tissue collection. CNS, central nervous system. **b**, **c**, Survival of mice at Harvard BRI ($C9orf72^{+/+}$, $n = 55$; $C9orf72^{+/-}$, $n = 114$; $C9orf72^{-/-}$, $n = 62$) (**b**) or the Broad Institute ($C9orf72^{+/+}$, $n = 22$; $C9orf72^{+/-}$, $n = 36$; $C9orf72^{-/-}$, $n = 23$) (**c**) (Gehan–Breslow–Wilcoxon). NS, not significant. **d**–**g**, Age-matched (48-week-old) mice reared at Harvard BRI ($C9orf72^{+/+}$, $n = 12$; $C9orf72^{+/-}$, $n = 13$; $C9orf72^{-/-}$, $n = 10$) or the Broad Institute ($C9orf72^{+/+}$, $n = 12$; $C9orf72^{+/-}$, $n = 18$; $C9orf72^{-/-}$, $n = 11$) were assessed for spleen weight (**d**), blood neutrophil count (**e**), blood platelet count measured at 0 °C (**f**) and plasma anti-double-stranded (ds)DNA antibody activity (**g**). In **d**–**g**, one-way ANOVA with Sidak's multiple comparisons. Each dot represents one mouse.

facility (hereafter referred to as *C9orf72(Harvard)* mice) (Fig. 1a). To assess the reproducibility of the original findings at Harvard, we aged an independent cohort of *C9orf72(Harvard)* mice ($C9orf72(Harvard)^{+/+}$, $n = 55$; $C9orf72(Harvard)^{+/-}$, $n = 114$; $C9orf72(Harvard)^{-/-}$, $n = 62$) and again found that $C9orf72(Harvard)^{+/-}$ mice (Gehan–Breslow–Wilcoxon $P = 0.0460$) and $C9orf72(Harvard)^{-/-}$ mice (Gehan–Breslow–Wilcoxon $P < 0.0001$) were at an increased risk of premature mortality (Fig. 1b). The causes of death in these mice—which included cervical lymphadenopathy, wasting and severe ataxia—were indistinguishable from those that were observed previously[7], and were closely tied to their underlying autoimmune condition (Extended Data Fig. 2a, b). By contrast, we observed no early mortality or motor behaviour deficit in either heterozygous or homozygous mutant mice at the Broad Institute ($C9orf72(Broad)^{+/+}$ $n = 22$, $C9orf72(Broad)^{+/-}$ $n = 36$, $C9orf72(Broad)^{-/-}$ $n = 23$) (Fig. 1c, Extended Data Fig. 2c). As a result, $C9orf72^{-/-}$ mice were significantly more likely to die prematurely when reared at Harvard than at the Broad Institute (Gehan–Breslow–Wilcoxon test, $P = 0.0179$). We therefore conclude that signals from the environment can be significant modifiers of lifespan when *C9orf72* function declines.

To determine whether the improved survival that we observed in *C9orf72(Broad)* mice was associated with a diminution of inflammatory and autoimmune endophenotypes[7], we jointly analysed age-matched mice reared at each facility (Fig. 1d–g, Extended Data Fig. 2d, e). As previously reported[7], *C9orf72(Harvard)* mice exhibited autoimmune and inflammatory phenotypes, including significantly elevated levels of IL-23, IL-10, IL-22, G-CSF, IL-17a, TNF, IFNγ, IL-1β and IL-12p70 ($P < 0.05$) (Extended Data Fig. 2e) as well as splenomegaly ($P < 0.0001$) (Fig. 1d), neutrophilia ($P < 0.0001$) (Fig. 1e), pseudothrombocytopenia ($P < 0.0001$) (Fig. 1f, Extended Data Fig. 2f, g) and development of auto-antibodies ($P < 0.0001$) (Fig. 1g). Notably and in every case, these inflammatory phenotypes were significantly reduced in $C9orf72(Broad)^{-/-}$ mice relative to their *C9orf72(Harvard)* mutant counterparts (Fig. 1d–g). In fact, the reduction of inflammation in the pro-survival Broad Institute environment was sufficiently reduced that many inflammatory phenotypes that we routinely observed in mutant mice at Harvard were no longer significantly different between $C9orf72^{-/-}$ and $C9orf72^{+/+}$ mice at the Broad Institute. It is notable that the few phenotypes that remained significantly different between $C9orf72(Broad)^{-/-}$ and $C9orf72(Broad)^{+/+}$ mice, such as modest splenomegaly (one-way analysis of variance (ANOVA) with Sidak's multiple comparisons, $P = 0.0004$), were those that have been most widely reported[6,13,14]. Thus, an environment that improved survival also ameliorated the underlying inflammatory and autoimmune disease found in *C9orf72* mutant mice.

Antibiotics prevent inflammation

We next considered variables between the two environments that might have contributed to such marked differences in the severity of mutant phenotypes. We found that diet, light cycle and many other features of the two environments were similar. However, a review of microbial screening reports from the two facilities indicated that murine norovirus (Fisher's exact test, $P = 0.0140$), *Helicobacter* spp. (Fisher's exact test, $P < 0.0001$), *Pasteurella pneumotropica* (Fisher's exact test, $P = 0.0070$) and *Tritrichomonas muris* (Fisher's exact test, $P < 0.0001$) were significantly more common in *C9orf72(Harvard)* mice than in *C9orf72(Broad)* mice (Supplementary Table 1). It is important to note that the differences between the two colonies were well within norms for Assessment and Accreditation of Laboratory Animal Care processes. The differential components of the microflora that we found at Harvard are not generally considered pathogenic, consistent with the normal health and lifespan of control mice in that environment[7] (Fig. 1b). However, *Helicobacter* spp. have previously been suggested to have immune-stimulating properties[10], which raises the possibility that changes in gut microflora between the two environments might underlie the increased rate of mortality and inflammatory phenotypes that we found in *C9orf72(Harvard)* mutant mice.

To learn whether the resident microflora contributed to the inflammation and autoimmunity seen in *C9orf72(Harvard)* mutant mice, we weaned new *C9orf72(Harvard)* mice ($C9orf72(Harvard)^{+/+}$, $n = 14$; $C9orf72(Harvard)^{-/-}$, $n = 22$) and administered either vehicle or broad-spectrum antibiotics before the onset of inflammatory disease (day 30), then monitored related phenotypes for 200 days (Fig. 2a). As expected, antibiotics significantly reduced the abundance and diversity of bacterial species (including *Helicobacter* spp.), without affecting levels of murine norovirus. The guts of vehicle-treated control mice were largely unaltered (Fig. 2b, Extended Data Fig. 3a). We found that vehicle had no effect on the development of either inflammatory or autoimmune phenotypes in $C9orf72(Harvard)^{-/-}$ mice, including cytokine storm (Extended Data Fig. 3b), neutrophilia (Fig. 2c), pseudothrombocytopenia (Fig. 2d), autoimmunity (Fig. 2e) and splenomegaly (Fig. 2f, Extended Data Fig. 3c). By contrast, providing lifelong antibiotics treatment to $C9orf72(Harvard)^{-/-}$ mice completely suppressed the emergence of all of these phenotypes (Fig. 2c–f, Extended Data Fig. 3b–i). Thus, our experiments suggest that signals derived from gut bacteria promote inflammation and autoimmunity when *C9orf72* function is diminished. However, we found that chronic administration of antibiotics resulted in previously reported health consequences (including hepatoxicity)[17], which prevented us from assessing behavioural and survival outcomes.

We next asked whether the acute suppression of gut microbiota could ameliorate inflammatory and autoimmune phenotypes after their establishment in *C9orf72(Harvard)* mutant mice. To this end, we obtained another independent cohort of *C9orf72(Harvard)* mice ($C9orf72(Harvard)^{+/+}$, $n = 25$; $C9orf72(Harvard)^{-/-}$, $n = 24$; day 250), demonstrated these mice displayed the expected inflammatory phenotypes

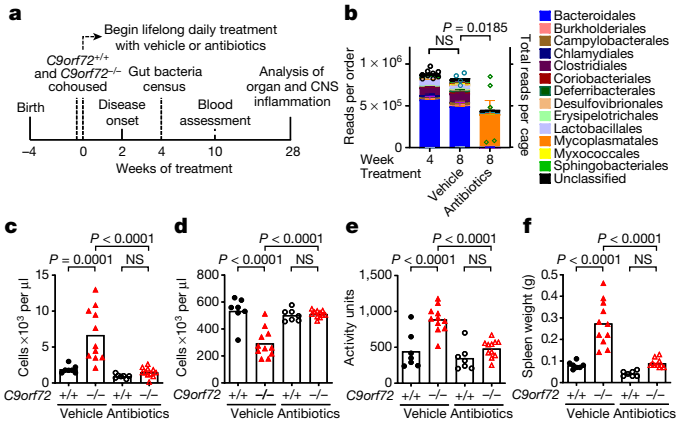

Fig. 2 | Lifelong suppression of gut microflora prevents inflammation and autoimmunity in *C9orf72* LOF mice. a, Male and female *C9orf72(Harvard)*$^{+/+}$ and *C9orf72(Harvard)*$^{-/-}$ neo-deleted mice of weaning age were cohoused by treatment group, then administered vehicle (*C9orf72(Harvard)*$^{+/+}$, $n = 7$; *C9orf72(Harvard)*$^{-/-}$, $n = 11$) or antibiotics (*C9orf72(Harvard)*$^{+/+}$, $n = 7$; *C9orf72(Harvard)*$^{-/-}$, $n = 11$) daily for life. **b**–**f**, Mice were assessed for gut microbial composition at 4 weeks (**b**) and blood measurements at 8 weeks (**c**–**e**), and killed for organ and central nervous system assessment at 28 weeks (**f**). **b**, 16S rDNA sequencing of bacteria diversity in faeces. Each dot represents total sequencing reads per cage. One-way ANOVA with Dunnett's multiple comparisons. **c**, Blood neutrophil count. **d**, Blood platelet count measured at 0 °C. **e**, Plasma anti-dsDNA antibody activity. **f**, Spleen weight. In **c**–**f**, one-way ANOVA with Sidak's multiple comparisons. Each dot represents one mouse.

relative to control mice and showed that they exhibited poor performance on the accelerating rotarod (Fig. 3a–d, Extended Data Fig. 4a). Then, we began acute administration of broad-spectrum antibiotics and monitored associated phenotypes over the course of 60 days. We found that this treatment significantly reduced each of the inflammatory and autoimmune phenotypes in mutant mice (Fig. 3b–d), including splenomegaly ($P = 0.0002$) (Extended Data Fig. 4c, d) and improved rotarod performance ($P = 0.0398$) (Extended Data Fig. 4a). By contrast, treatment with vehicle had no effect on these measures (Fig. 3b–d, Extended Data Fig. 4a–d).

Faecal transplants mitigate inflammation

To more directly investigate whether the phenotypic improvements were due to the microbial communities of the gut (rather than unrelated consequences of antibiotics treatment), we performed faecal transplant experiments. We produced another cohort of *C9orf72(Harvard)* mice (*C9orf72(Harvard)*$^{+/+}$, $n = 27$; *C9orf72(Harvard)*$^{-/-}$, $n = 32$; day 100) and demonstrated that these mice displayed the expected inflammatory phenotypes relative to control mice. We then suppressed the gut microflora of these mice with transient antibiotic treatment, and transplanted with faeces from either the pro-inflammatory (Harvard BRI) or pro-survival (Broad Institute) environment (Fig. 3e). Transplantation of pro-survival gut microflora significantly improved each of the inflammatory and autoimmune phenotypes (Fig. 3f–h, Extended Data Fig. 4e). By contrast, transplant with microflora from the pro-inflammatory facility did not improve these measures, which suggests that the benefits we observed when transplanting faeces from the protective environment were not merely due to the brief antibiotic treatment that enabled microbial engraftment. Therefore, our studies establish that the inflammatory and autoimmune disease that underlies premature mortality in *C9orf72(Harvard)* mutant mice can be therapeutically prevented, and that signals from particular gut microbiota help to maintain this disease.

Profiling gut bacteria

To identify the bacterial species of the gut that are associated with severe phenotypes in *C9orf72(Harvard)* mutant mice, we surveyed the composition of faeces from two pro-inflammatory environments in which the mutant mice perished[7,12], as well as from one previously published[6] and one additional pro-survival environment (Fig. 3i). Principal component analysis readily separated samples from the four environments, with the largest principal component (principal component 1, 28.7% of variance) separating the two pro-inflammatory environments from the two pro-survival environments (Fig. 3j). Deeper investigation of this axis of variance revealed a shared significant decrease in α-diversity in the two pro-inflammatory environments, and unsupervised hierarchical clustering demonstrated that samples from the pro-inflammatory environments showed β-diversity disparate from that in pro-survival environments (Fig. 3k, Extended Data Fig. 5f). Exemplifying these considerable differences in community structure, 62 of 301 bacterial species we identified (20.6%) were significantly altered in their abundance when jointly comparing the two pro-survival environments to the two pro-inflammatory environments ($P < 0.0002$) (Extended Data Fig. 5a–e). Consistent with initial observations (Supplementary Table 1), *Helicobacter* spp. were found in both of the pro-inflammatory environments (Extended Data Fig. 5g, h, Supplementary Fig. 1) but were absent in pro-survival environments.

We next characterized the extent of microbial reconstitution in our faecal transplant recipients (Extended Data Fig. 6a–f). Hierarchical clustering of β-diversity revealed that the microbial composition in mice that received faecal transplants from the Broad Institute environment were more similar to faeces from mice housed at the Broad Institute than to faeces from mice housed at Harvard BRI or faeces from mice that received faecal transplants from the Harvard environment (Extended Data Fig. 6d). Analysis of individual bacteria similarly supported the success of our transplants: 85% (199 out of 234) of bacterial species identified in faeces from mice housed at Harvard BRI being detected in mice that received faecal transplants from the Harvard environment, and 75% (178 out of 236) of bacterial species identified in faeces from mice housed at the Broad Institute detected in mice that received faecal transplants from the Broad Institute environment (Extended Data Fig. 6f). Semi-quantitative PCR for *Helicobacter* spp. ribosomal (r)DNA further confirmed the reconstitution of Harvard-specific microorganisms in the recipients of faecal transplants from the Harvard environment, and their elimination from the recipients of faecal transplants from the Broad Institute environment (Extended Data Fig. 5i, Supplementary Fig. 1).

Gut components regulate myeloid cytokines

To mechanistically explore how varied faecal components in separate environments alter cytokine burden and autoimmunity in *C9orf72*$^{-/-}$ mice, we stimulated bone-marrow-derived macrophages from *C9orf72(Harvard)* mice with chemical analogues of microbial components and found that both *C9orf72(Harvard)*$^{+/-}$ and *C9orf72(Harvard)*$^{-/-}$ bone-marrow-derived macrophages released higher levels of several pro-inflammatory cytokines than *C9orf72(Harvard)*$^{+/+}$ control cells in response to bacterial lipopeptide, single-stranded (ss)RNA and ssDNA (Extended Data Fig. 7a–c). Given these findings, we next asked whether faecal material from mice housed at Harvard BRI contained higher levels of innate-immune stimulating factors than faeces from mice at the Broad Institute. To this end, we individually administered normalized concentrations of faecal Eubacteria from both institutions to *C9orf72(Harvard)*$^{-/-}$ and *C9orf72(Harvard)*$^{+/+}$ bone-marrow-derived macrophages. We found that *C9orf72*$^{-/-}$ bone-marrow-derived macrophages produced significantly higher levels of TNF when exposed to faecal material from Harvard BRI than when exposed to faeces from the Broad Institute (Extended Data Fig. 7d). In addition, serial dilutions

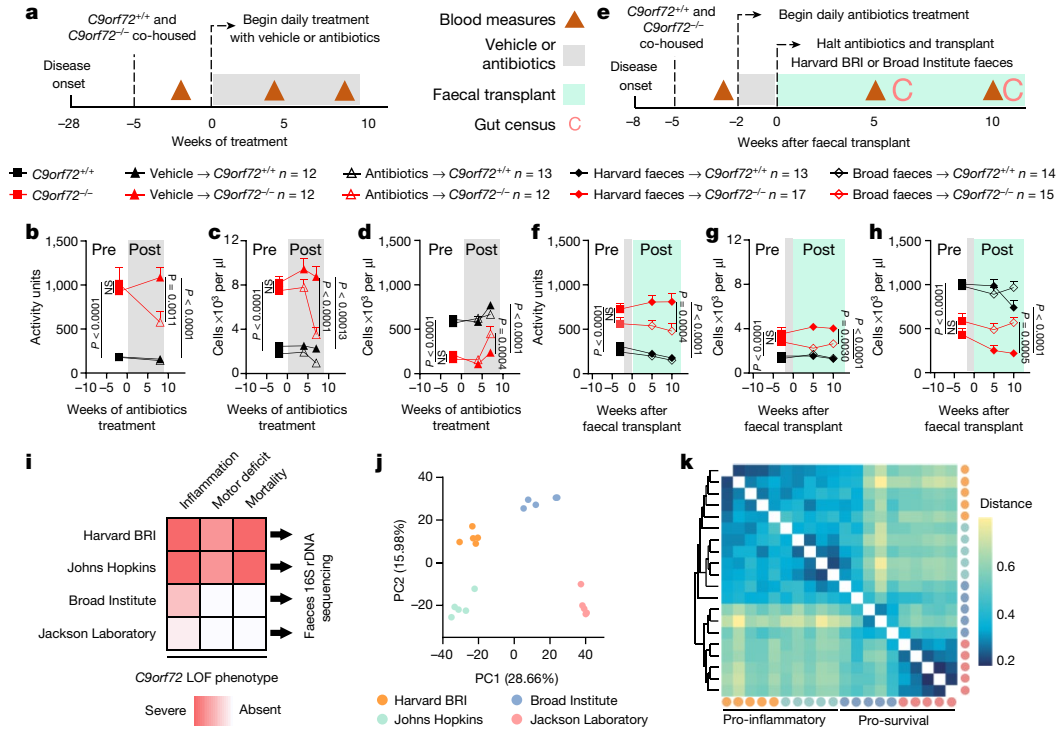

Fig. 3 | Gut bacteria propagates inflammation and autoimmunity in *C9orf72* LOF mice. a, Age-matched (36-week-old) female *C9orf72(Harvard)*$^{+/+}$ and *C9orf72(Harvard)*$^{-/-}$ neo-deleted mice were cohoused by treatment group, then administered vehicle (*C9orf72(Harvard)*$^{+/+}$, $n = 12$; *C9orf72(Harvard)*$^{-/-}$, $n = 12$) or antibiotics (*C9orf72(Harvard)*$^{+/+}$, $n = 13$; *C9orf72(Harvard)*$^{-/-}$, $n = 12$) daily. **b**–**d**, These mice were then assessed for plasma anti-dsDNA antibody activity (**b**), blood neutrophil count (**c**) and blood platelet count measured at 0 °C (**d**). **e**, Age-matched (13-week-old) female *C9orf72(Harvard)*$^{+/+}$ and *C9orf72(Harvard)*$^{-/-}$ neo-deleted mice were cohoused by treatment group, administered antibiotics for two weeks, and then gavaged with faeces from the Harvard BRI environment (*C9orf72(Harvard)*$^{+/+}$, $n = 13$; *C9orf72(Harvard)*$^{-/-}$, $n = 17$) or Broad Institute environment (*C9orf72(Harvard)*$^{+/+}$, $n = 14$; *C9orf72(Harvard)*$^{-/-}$, $n = 15$). **f**–**h**, These mice were then assessed for plasma anti-dsDNA antibody activity (**f**), blood neutrophil count (**g**) and blood platelet count measured at 0 °C (**h**). **i**–**k**, Faecal pellets ($n = 5$ each) from two pro-inflammatory environments (Harvard BRI and Johns Hopkins) and two pro-survival environments (Broad Institute and Jackson Laboratory) were subjected to 16S rDNA sequencing (**i**), and then assessed by principal component (PC) analysis (**j**) and Bray–Curtis dissimilarity matrix of β-diversity (**k**). In **b**–**d**, **f**–**h**, one-way ANOVA with Sidak's multiple comparisons. Each dot represents one mouse.

revealed that a combination of faeces from Harvard BRI and a *C9orf72*$^{-/-}$ genotype leads to TNF release at the lowest faecal concentrations (Extended Data Fig. 7d).

Environment governs neuro-inflammation

Neuro-inflammation is a pathological hallmark of ALS and FTD associated with mutations in *C9ORF72*[18,19], with substantial infiltration of peripheral immune cells noted in the spinal cord of patients with ALS[20,21]. We used the pan-haematopoietic marker CD45 to distinguish CD45^{mid} resident microglia from peripherally derived CD45^{high} cells[22] and found that infiltrating cells were present at sites of focal inflammation within the spinal cord parenchyma of *C9orf72(Harvard)*$^{-/-}$ mice (Fig. 4a, Extended Data Fig. 8a–h, Supplementary Videos 1, 2). Mass cytometry analysis revealed that the CD45^{high} cells that infiltrated the spinal cord were mostly CD11b^{+}Ly6C^{+}Ly6G^{+}CD39^{-} neutrophils and CD3e^{+} T cells (Extended Data Fig. 8a–f; gating strategy is in Supplementary Information). Notably, lifelong suppression of gut microflora with antibiotics prevented the accumulation of infiltrating myeloid cells within the spinal cord of *C9orf72(Harvard)*$^{-/-}$ mice (Fig. 4b, c).

In addition to infiltrating peripheral immune cells, there are also substantial changes to resident microglia in the nervous systems of patients with ALS or FTD[23]. Previous studies[6,8,9,24] have implicated C9orf72 and its interactor SMCR8 in regulation of endolysosomal trafficking and autophagy, particularly in myeloid derivatives. We found that microglia from the spinal cord of *C9orf72(Harvard)*$^{-/-}$ mice expressed higher levels of the lysosome-associated proteins LAMP1[6] (Extended Data Fig. 9a, Supplementary Videos 3, 4) and cathepsin B (Extended Data Fig. 9b, Supplementary Videos 5, 6). Lifelong suppression of gut microbiota did not significantly decrease LAMP1 or cathepsin B levels in *C9orf72(Harvard)*$^{-/-}$ microglia (Extended Data Fig. 9c, d), which suggests that *C9orf72* regulates lysosomal constituents independently from microbial signals.

To examine the activation status of resident microglia in *C9orf72(Harvard)* mutant mice and to ask whether microglial activation might be altered by signals from the microbiota, we measured levels of the pattern recognition receptor dectin 1, the chemokine receptor CCR9 and the lipoprotein lipase LPL, which have previously been associated with pro-inflammatory microglial states[25–27]. Consistent with the notion that microglia become activated when *C9orf72* levels decline, we found that dectin 1 and CCR9 were enriched in microglia from *C9orf72(Harvard)*$^{-/-}$ mice (Fig. 4d–f, Extended Data Fig. 9e–g, Supplementary Videos 7, 8). Importantly, dectin 1 and CCR9 expression were significantly reduced in microglia from *C9orf72(Harvard)* mutant mice with gut microflora that was chronically suppressed with antibiotics (Fig. 4d–f). These results demonstrate that when *C9orf72* function is reduced, peripheral immune cells can infiltrate the spinal cord, where they associate with sites of neuro-inflammation, and that treatment with antibiotics, which suppresses the microbiota, modulates both infiltration and microglial activation.

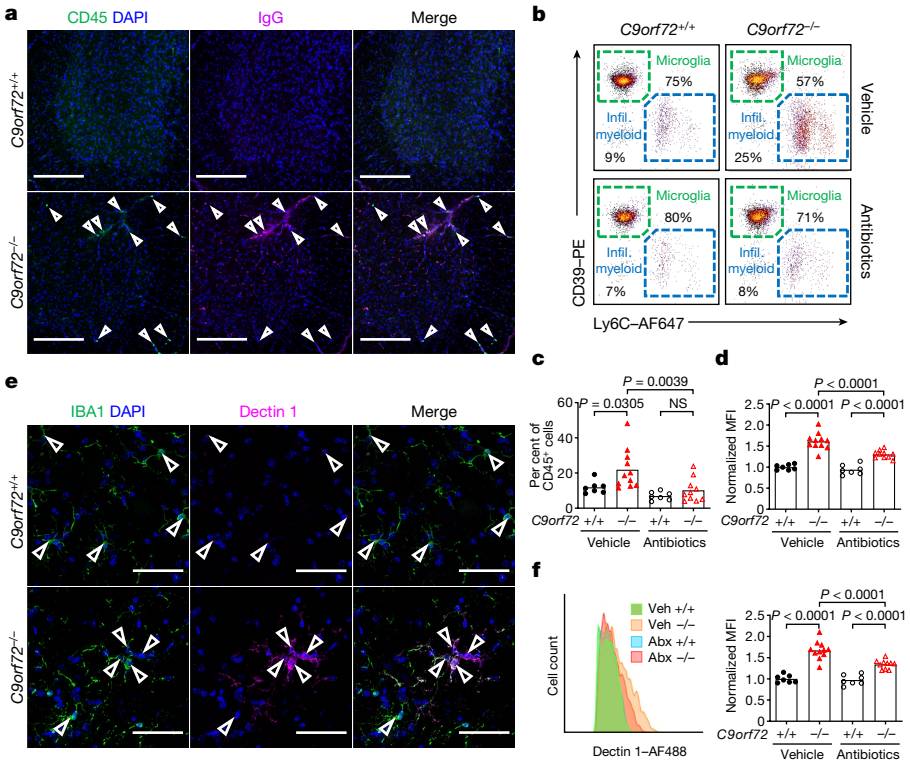

Fig. 4 | Gut microflora promotes myeloid cell infiltration and microgliosis in *C9orf72* LOF spinal cord. a, Orthogonal projection of CD45 and mouse immunoglobulin G (IgG) in lumbar spinal cord of 55-week-old *C9orf72(Harvard)* neo-deleted mice (*C9orf72(Harvard)*$^{+/+}$, $n = 3$; *C9orf72(Harvard)*$^{-/-}$, $n = 3$), showing cells infiltrating the lumbar spinal cord. Scale bars, 200 µm. **b**, Representative gating of CD45^{+}CD11b^{+} cells from spinal cord of *C9orf72(Harvard)* mice in Fig. 2. Infil., infiltrating. **c**, Quantification of CD45^{high}CD11b^{+}Ly6C^{+} myeloid cells infiltrating the spinal cord, shown in **b**. **d**, Quantification of CCR9 expression on CD45^{mid}CD11b^{+}CD39^{+} microglia from the spinal cord of *C9orf72(Harvard)* mice, shown in Fig. 2. MFI, mean fluorescence intensity. **e**, Orthogonal projection of dectin 1 in IBA1^{+} microglia in lumbar spinal cord from 55-week-old *C9orf72(Harvard)* neo-deleted mice (*C9orf72(Harvard)*$^{+/+}$, $n = 3$; *C9orf72(Harvard)*$^{-/-}$, $n = 3$). Scale bars, 50 µm. **f**, Dectin 1 in CD45^{mid}CD11b^{+}CD39^{+} microglia from spinal cord of *C9orf72(Harvard)* mice in Fig. 2. +/+, *C9orf72(Harvard)*$^{+/+}$; −/−, *C9orf72(Harvard)*$^{-/-}$; abx, antibiotics-treated; veh, vehicle-treated. In **c**, **d**, **f**, one-way ANOVA with Sidak's multiple comparisons. Each dot represents one mouse.

Discussion

Our results indicate that when *C9orf72* function declines, the environment generally—and the gut microbiota specifically—become potent modifiers of whether autoimmunity, neural inflammation, motor deficits and premature mortality occur. The effect of environment and accompanying changes in microbial microflora are so strong in this mouse model that in one environment, inflammatory disease and death were highly penetrant phenotypes, whereas in another they were essentially absent. We therefore provide the probable explanation for the considerable phenotypic variation that has been observed across groups studying this *C9orf72* LOF allele in mice[6,7,12,13]. These conclusions are important because they re-emphasize that the 50% reduction in the levels of *C9ORF72* found in patients with ALS or FTD who have mutations in *C9ORF72* are a credible cause for the neural inflammation that are characteristic in their condition. Most provocatively, our findings also suggest that variance in microbiota could explain why some carriers of the *C9ORF72* mutation develop ALS or FTD, or overt inflammatory conditions such as lupus[15,16], while others do not.

It should be re-emphasized that the microorganisms present in the environments we studied here are not considered mouse pathogens per se, and that their abundances were within the scope found in comparable institutions[28]. Importantly, the environmental conditions that triggered severe phenotypes in our *C9orf72(Harvard)* mice were reproducible elsewhere. Previous reports[7,12] have noted a relationship between the reduction in *C9orf72* function and an increased rate of premature mortality comparable to that described here. It is notable that these two pro-inflammatory environments were most similar in their microbial constituents and also shared many microorganisms that were not present in the two pro-survival locations we surveyed. Given the large number of species that we found significantly differ in their abundance between pro-inflammatory and pro-survival environments (Fig. 3i, Extended Data Fig. 5c), future studies will be needed to elucidate the relative contribution of individual bacterial species to variation in the inflammatory and autoimmune phenotypes we report here. However, microorganism-by-microorganism analysis of varying environments and our transplant mice would seem to rule out the previously reported protective effects of *Akkermansia muciniphila*[29,30] (Extended Data Fig. 6f) and potential inflammatory influences of *T. muris* (Extended Data Fig. 5e).

It is increasingly appreciated that gut microorganisms alter the maturation and function of microglia[31], can influence the activity of neurons in the central nervous system[32] and contribute to neuro-inflammation and neuropathology in models of Alzheimer's[33] and Parkinson's disease[34]. However, only initial surveys of the gut microbiota have been reported in patients with neurological conditions[35] and, thus far, results from initial studies in patients with ALS have been mixed[36,37]. One study has reported significant differences between the microbial constituencies of patients with ALS and controls[36], whereas another found no clear distinctions[37]. Given the genetic heterogeneity exhibited within patients with ALS, it is perhaps not surprising that early studies have not reached consensus.

Consistent with the idea there are complex interactions between the germline genotype of a patient and their gut microflora in ALS, it

was recently reported that *SOD1*-transgenic mice displayed a faster decline when bacterial load was reduced, which was linked to reduced bacterial production of nicotinamide[29]. Although we cannot rule out the presence of protective microorganisms in some environments, our studies suggest that lowering the bacterial load in *C9orf72*-mutant mice was in aggregate protective, probably by reducing the exposure of their genetically sensitized innate immune response to inflammatory factors derived from microorganisms. In sum, our studies suggests that the microbiome may be an important governor of the onset and progression of neurological disease in patients with *C9ORF72* mutations, including those experiencing autoimmune and inflammatory conditions before a diagnosis of ALS or FTD[15,16]. To test this idea, a key future experiment will be to identify *C9ORF72* repeat expansion carriers within families known to be predisposed to developing ALS or FTD, and to determine whether the gut microbiota differs between individuals that remain healthy and those that acquire the conditions.

Online content

Any methods, additional references, Nature Research reporting summaries, source data, extended data, supplementary information, acknowledgements, peer review information; details of author contributions and competing interests; and statements of data and code availability are available at https://doi.org/10.1038/s41586-020-2288-7.

1. DeJesus-Hernandez, M. et al. Expanded GGGGCC hexanucleotide repeat in noncoding region of *C9ORF72* causes chromosome 9p-linked FTD and ALS. *Neuron* **72**, 245–256 (2011).
2. Majounie, E. et al. Frequency of the *C9orf72* hexanucleotide repeat expansion in patients with amyotrophic lateral sclerosis and frontotemporal dementia: a cross-sectional study. *Lancet Neurol.* **11**, 323–330 (2012).
3. Mori, K. et al. The *C9orf72* GGGGCC repeat is translated into aggregating dipeptide-repeat proteins in FTLD/ALS. *Science* **339**, 1335–1338 (2013).
4. Ash, P. E. A. et al. Unconventional translation of *C9ORF72* GGGGCC expansion generates insoluble polypeptides specific to c9FTD/ALS. *Neuron* **77**, 639–646 (2013).
5. Donnelly, C. J. et al. RNA toxicity from the ALS/FTD *C9ORF72* expansion is mitigated by antisense intervention. *Neuron* **80**, 415–428 (2013).
6. O'Rourke, J. G. et al. *C9orf72* is required for proper macrophage and microglial function in mice. *Science* **351**, 1324–1329 (2016).
7. Burberry, A. et al. Loss-of-function mutations in the *C9ORF72* mouse ortholog cause fatal autoimmune disease. *Sci. Transl. Med.* **8**, 347ra93 (2016).
8. Nassif, M., Woehlbier, U. & Manque, P. A. The enigmatic role of C9ORF72 in autophagy. *Front. Neurosci.* **11**, 442 (2017).
9. Shi, Y. et al. Haploinsufficiency leads to neurodegeneration in *C9ORF72* ALS/FTD human induced motor neurons. *Nat. Med.* **24**, 313–325 (2018).
10. Whary, M. T. & Fox, J. G. Natural and experimental *Helicobacter* infections. *Comp. Med.* **54**, 128–158 (2004).
11. Flannigan, K. L. & Denning, T. L. Segmented filamentous bacteria-induced immune responses: a balancing act between host protection and autoimmunity. *Immunology* **154**, 537–546 (2018).
12. Ugolino, J. et al. Loss of C9orf72 enhances autophagic activity via deregulated mTOR and TFEB signaling. *PLoS Genet.* **12**, e1006443 (2016).
13. Jiang, J. et al. Gain of toxicity from ALS/FTD-linked repeat expansions in *C9ORF72* is alleviated by antisense oligonucleotides targeting GGGGCC-containing RNAs. *Neuron* **90**, 535–550 (2016).
14. Atanasio, A. et al. *C9orf72* ablation causes immune dysregulation characterized by leukocyte expansion, autoantibody production, and glomerulonephropathy in mice. *Sci. Rep.* **6**, 23204 (2016).
15. Miller, Z. A. et al. Increased prevalence of autoimmune disease within C9 and FTD/MND cohorts. *Neurol. Neuroimmunol. Neuroinflamm.* **3**, e301 (2016).
16. Fredi, M. et al. *C9orf72* intermediate alleles in patients with amyotrophic lateral sclerosis, systemic lupus erythematosus, and rheumatoid arthritis. *Neuromolecular Med.* **21**, 150–159 (2019).
17. Stine, J. G. & Lewis, J. H. Hepatotoxicity of antibiotics: a review and update for the clinician. *Clin. Liver Dis.* **17**, 609–642, ix (2013).
18. Ransohoff, R. M. How neuroinflammation contributes to neurodegeneration. *Science* **353**, 777–783 (2016).
19. McCauley, M. E. & Baloh, R. H. Inflammation in ALS/FTD pathogenesis. *Acta Neuropathol.* **137**, 715–730 (2019).
20. Zhao, W., Beers, D. R. & Appel, S. H. Immune-mediated mechanisms in the pathoprogression of amyotrophic lateral sclerosis. *J. Neuroimmune Pharmacol.* **8**, 888–899 (2013).
21. Zondler, L. et al. Peripheral monocytes are functionally altered and invade the CNS in ALS patients. *Acta Neuropathol.* **132**, 391–411 (2016).
22. Zhang, G. X., Li, J., Ventura, E. & Rostami, A. Parenchymal microglia of naïve adult C57BL/6J mice express high levels of B7.1, B7.2, and MHC class II. *Exp. Mol. Pathol.* **73**, 35–45 (2002).
23. Lall, D. & Baloh, R. H. Microglia and C9orf72 in neuroinflammation and ALS and frontotemporal dementia. *J. Clin. Invest.* **127**, 3250–3258 (2017).
24. Zhang, Y. et al. The C9orf72-interacting protein Smcr8 is a negative regulator of autoimmunity and lysosomal exocytosis. *Genes Dev.* **32**, 929–943 (2018).
25. Li, H. et al. Different neurotropic pathogens elicit neurotoxic CCR9- or neurosupportive CXCR3-expressing microglia. *J. Immunol.* **177**, 3644–3656 (2006).
26. Krasemann, S. et al. The TREM2–APOE pathway drives the transcriptional phenotype of dysfunctional microglia in neurodegenerative diseases. *Immunity* **47**, 566–581.e9 (2017).
27. Keren-Shaul, H. et al. A unique microglia type associated with restricting development of Alzheimer's disease. *Cell* **169**, 1276–1290.e17 (2017).
28. Nilsson, H.-O. et al. High prevalence of *Helicobacter* species detected in laboratory mouse strains by multiplex PCR-denaturing gradient gel electrophoresis and pyrosequencing. *J. Clin. Microbiol.* **42**, 3781–3788 (2004).
29. Blacher, E. et al. Potential roles of gut microbiome and metabolites in modulating ALS in mice. *Nature* **572**, 474–480 (2019).
30. Zhai, R. et al. Strain-specific anti-inflammatory properties of two *Akkermansia muciniphila* strains on chronic colitis in mice. *Front. Cell. Infect. Microbiol.* **9**, 239 (2019).
31. Erny, D. et al. Host microbiota constantly control maturation and function of microglia in the CNS. *Nat. Neurosci.* **18**, 965–977 (2015).
32. Olson, C. A. et al. The gut microbiota mediates the anti-seizure effects of the ketogenic diet. *Cell* **173**, 1728–1741.e13 (2018).
33. Harach, T. et al. Reduction of Abeta amyloid pathology in APPPS1 transgenic mice in the absence of gut microbiota. *Sci. Rep.* **7**, 41802 (2017).
34. Sampson, T. R. et al. Gut microbiota regulate motor deficits and neuroinflammation in a model of Parkinson's disease. *Cell* **167**, 1469–1480.e12 (2016).
35. Tremlett, H., Bauer, K. C., Appel-Cresswell, S., Finlay, B. B. & Waubant, E. The gut microbiome in human neurological disease: a review. *Ann. Neurol.* **81**, 369–382 (2017).
36. Fang, X. et al. Evaluation of the microbial diversity in amyotrophic lateral sclerosis using high-throughput sequencing. *Front. Microbiol.* **7**, 1479 (2016).
37. Brenner, D. et al. The fecal microbiome of ALS patients. *Neurobiol. Aging* **61**, 132–137 (2018).

Methods

Mice

All experimental procedures were approved by the Institutional Animal Care and Use Committee of Harvard University and the Broad Institute, and were in compliance with all relevant ethical regulations. The KOMP and neo-deleted *C9orf72* loss of function strains were generated as previously described[7]. Mice were housed with nestlet bedding, red hut for enrichment, provided water ad libitum and fed ad libitum either with Prolab Isopro RMH 3000 (Harvard BRI) or with PicoLab Rodent Diet 20 (Broad Institute) and kept on a 12-h light–dark cycle. Embryo re-derivation was performed by collecting embryos from super-ovulated *C9orf72*$^{+/-}$ females, washing embryos, then surgical transfer using an aseptic technique into the reproductive tract of pseudopregnant recipient females. For experiments involving antibiotics, mice were cohoused for at least a week before initiation of dosing. Mice were administered either vehicle (water) or a freshly prepared cocktail of four antibiotics including ampicillin sodium salt (200 mg/kg/d), neomycin trisulfate salt hydrate (200 mg/kg/d), metronidazole (200 mg/kg/d), and vancomycin hydrochloride from *Streptomyces orientalis* (100 mg/kg/d) (all from Sigma) administered by twice daily gavage. The number (*n*), sex and ages of the mice used in each study are described in figure legends or text. Power calculations (G*Power 3.1.9.2) using the mean and standard error of endophenotype data was used to estimate necessary cohort sizes for antibiotics and faecal transplant studies. Before administration of antibiotics, mice were assessed for systemic inflammatory measures and mice were allocated into groups so that no significant differences were present before treatment initiation.

Motor behaviour

Naive mice were trained on the rotarod at constant speed of 4 rpm for 300 s at least 1 d before competitive assessment. For performance trials, the rotarod accelerated from 4 to 40 rpm over 300 s using Ugo Basile mouse RotaRod NG (Harvard FAS BRI) or Panlab Rota Rod (Broad Institute). Each trial day consisted of 3 tests per mouse, with each test separated by at least 20 min. The operator was blinded to mouse genotype during trials.

Faecal transplantation

Using sterilized forceps, donor faecal pellets were collected directly from the anus, or donor upper and lower intestinal contents were isolated from euthanized mice and immediately frozen on dry ice. Recipient mice received antibiotics twice daily by gavage for two weeks, then a two day secession of antibiotics, then faecal transplantation once per day for two days. Faecal pellets and intestinal contents from donor mice were weighed, pooled, diluted to 200 mg/ml in degassed PBS and administered by oral gavage to recipient mice at 2 mg faeces per g of body weight. All cage changes were performed in HEPA filtered hoods with freshly autoclaved cages, bedding and enrichment.

Blood and cytokine measures

Peripheral blood was collected via mandible puncture into EDTA-coated tubes. Blood counts were assessed using a Hemavet (Abaxis). Samples were then centrifuged to pellet cells and plasma was collected from the supernatant. Plasma was diluted 1:2 for luminex-based multiplexed fluorescence assay to assess 36 cytokines and chemokines. Plasma was diluted 1:200 to assess mouse anti-dsDNA total IgG autoantibodies (Alpha Diagnostic International).

Tissue preparation

Mice were anaesthetized with isoflurane followed by transcardial perfusion with HBSS supplemented with 10 U/ml heparin. Spleens were dissociated by repeated trituration with a glass pipetman in HBSS, subjected to 10-min RBC lysis (eBioscience), washed in autoMACS (Miltenyi), filtered (40 μm) and counted using a Countess (Invitrogen) for antibody staining. For flow cytometry and mass cytometry of the central nervous system, spinal cords were digested by papain and DNase diluted in EBSS (Worthington) for 10 min at 37 °C, triturated with a glass pipetman to generate large tissue chunks, and then allowed to digest for 20 min at 37 °C. DMEM supplemented with glutamax was added, samples triturated to single cells, ovomucoid (Worthington) and DNase diluted in EBSS added to inhibit protease activity, cells filtered, washed in autoMACS buffer, and pelleted at 500*g* for 15 min at 4 °C. Cell pellets were brought up in isotonic Percol Plus (Sigma) diluted to 30% in autoMACS and spun for 15 min at room temperature with no brake. Floating myelin was gently removed using plastic transfer pipette. Cell pellets were resuspended, filtered, washed in autoMACS and re-pelleted at 4 °C. Cells were fixed in 4% paraformaldehyde (PFA) (Electron Microscopy Sciences) either before or after antibody staining depending on need. Samples were collected on a BD LSRII or Helios mass cytometer. Data were analysed using FlowJo and/or Cytobank. For immunofluorescence experiments, following HBSS perfusion, mice were perfused with 4% PFA and central nervous system tissue was post-fixed in 4% PFA overnight at 4 °C. The next day, samples were washed with PBS overnight at 4 °C. Tissue was submerged in 30% sucrose for 2 d. After cryoprotection, lumbar regions were mounted in OCT and cryostat-sectioned at 30 μm.

Immunofluorescence

Spinal cord sections were washed three times in PBS to remove residual OCT. Sections were incubated in a blocking solution (10% donkey serum, 0.1M glycine, 0.1% Tween20 or 0.3% Triton X100, PBS, Image-iT FX Signal Enhancer (Thermo)) for 1 h at room temperature. Following blocking, sections were incubated with primary antibodies for 2 d on a rocker at 4 °C. Primary antibodies include: rat CD11b–FITC 1:200 (M1/70, BioLegend), rabbit cathepsin B 1:400 (D1C7Y CST), rat CD45-488 1:200 (30-F11 BioLegend), guinea pig IBA1 1:500 (234004 Synaptic Systems), rat LAMP1 1:200 (1D4B SCB), rat CCR9–FITC (9B1 BioLegend), rat Dectin 1/CLEC7A (mabg-mdect Invivogen) and mouse LPL (ab21356 Abcam). Sections were then washed with 0.1% Tween20 in PBS (for stains with CD11b, CD45, CCR9, and cathepsin B) or 0.3% TritonX100 in PBS (for stains with IBA1, LAMP1, CLEC7A (dectin 1) and LPL) at least 5 times. Secondary antibodies include: donkey-anti-rat-AlexaFluor-488, -mouse IgG-555, -rabbit-555, -rabbit-647, -rat-647, -guinea pig-647, all 1:500 dilution (Invitrogen), for 2 h at room temperature. Sections were washed again, and mounted on microscope slides in Fluoromount for curing overnight. Spinal cords were imaged on a ZEISS LSM700 with either a 10× and 40× objective, or an Axio scan Z.1 at 20× objective. Images were stitched and processed on ZEISS ZEN 2.6 image processing software and Bitplane Imaris 9.2. All comparative stains between control and mutant mice were acquired using identical laser and microscope settings, and images were processed with viewer blinded to genotype.

Flow cytometry

Dissociated single cells were stained in autoMACS on ice using the following antibodies (BioLegend): CD45–BV421 or APC–Cy7 1:200 (30-F11), rabbit cathepsin B 1:100 (D1C7Y CST) and goat-anti-rabbit-AlexaFluor-488 1:500 (Invitrogen), CCR9–FITC 1:200 (9B1), F4/80–PE–Cy5 1:400 (BM8), CD11b–AlexaFluor-700 1:400 (M1/70 Invitrogen), LAMP1–APC–Cy7 1:400 (1D4B), TruStain FcX 1:250 (93), CD39–PE 1:400 (Duha59), Ly6G–PE–Cy7 1:600 (1A8), Ly6C–AlexaFluor-647 (HK1.4). To retrieve the cathepsin B epitope, fixed cells were slowly permeabilized in 90% methanol before staining for cathepsin B.

16S sequencing and PCR assays for rodent infectious agents

DNA was isolated by Powersoil (Qiagen) per the manufacturer's protocol, and recovery yield and DNA quality were determined by fluorometric analysis. DNA concentration was standardized and amplified using

16 s rRNA primers spanning the V3 and V4 regions (Illumina). Resulting amplified PCR products were analysed on a Bioanalyzer (Agilent Technologies), and then purified and amplified with primers containing unique sample nucleotide barcodes (Illumina). PCR products were analysed with the Bioanalyzer for product quality control and also by SYBR green PCR to determine the quantity. All samples were pooled and standardized to a final concentration of 4.0 nM representation for each sample. The 16S PCR product pool was denatured with sodium hydroxide then adjusted to 4.0 pM and combined with 5% PhiX control DNA before loading onto a sequencing flow cell (Illumina) with 300-bp paired ends and a unique molecular tag for each sample. Following the sequencing run, the sequence data were separated on the basis of the nucleotide bar code, and then compared to the Greengenes database[38]. Relative abundance, α-diversity, β-diversity and principal coordinate analysis were performed using QIIME analysis software[39]. PCR assays for rodent infectious agents were performed as described[40].

PCR

Faecal DNA was isolated from faecal pellets using QIAmp Fast DNA Stool Mini Kit (Qiagen). *Helicobacter* spp. 16S rDNA was amplified using primers 5′-CTATGACGGGTATCCGCC-3′ and 5′-ATTCCACCTACCTCTCCCA-3′. Total Eubacteria 16S rDNA was amplified using primers 5′-TCCTACGGGAGGCAGCAG-3′ and 5′-GGACTACCAGGGTATCTAATCCTGTT -3′. *T. muris* 28S rDNA was amplified using primers 5′-GCTTTTGCAAGCTAGGTCCC-3′ and 5′-TTTCTGATGGGGCGTACCAC -3′. RNA was isolated from tissue by dissociating cortex in Trizol LS (Thermo) using a pellet pestle and reverse transcriptase with iScript (Biorad). Quantitative PCR with reverse transcription as performed using SYBR (Biorad). *Ly6c* was amplified using primers 5′-TACTGTGTGCAGAAAGAGCTCAG-3′ and 5′- TTCCTTCTTTGAGAGTCCTCAATC-3′. *Gapdh* was amplified using primers 5′-TGCGACTTCAACAGCAACTC-3′ and 5′-GCCTCTC TTGCTCAGTGTCC-3′.

Bone-marrow-derived macrophages

Two femurs and tibias were stripped of musculature, flushed and cultured in IMDM supplemented with 10% FCS, NEAA, glutamax, penicillin–streptomycin and 20 ng/ml mouse M-CSF (PeproTech). The medium was changed on day 3 and cells plated for experiments after 6 days. Cells were plated at 4×10^4 cells per well of a 96-well plate, and allowed to attach overnight, followed by stimulation with microbial moieties (Invivogen), including Pam3csk4 (10–1,000 ng/ml; tlrl-pms), zymosan (1 μg/ml; tlrl-zyn), HMW poly(I:C) (10 μg/ml; tlrl-pic), LPS (10 ng/ml; tlrl-peklps), R848 (20 ng/ml; tlrl-r848), CpG ODN (25 μg/ml; tlrl-1826) or PGN (20 μg/ml; tlrl-pgnb3). For faecal stimulations, previously frozen faeces were thawed, diluted to 200 mg/ml in PBS, passed through a 40-μm filter, quick spun, and supernatant was collected and kept on ice. Bacterial DNA was isolated from each sample using QIAmp Fast DNA Stool Mini Kit (Qiagen) and total Eubacteria 16S rDNA abundance determined by qPCR. The more concentrated sample was diluted in PBS to normalize the relative Eubacteria abundance, which was confirmed again by bacterial DNA isolation and qPCR. Dilution curves were prepared for each normalized faecal sample and added to macrophage cultures. Penicillin–streptomycin was added to cultures after 2 h, then the medium was collected after 18 h for testing by TNF enzyme-linked immunosorbent assay at 1:2 and 1:10 dilution (BioLegend).

Statistics

Statistical calculations were performed using GraphPad prism 8.0. Tests between two groups used a two-tailed Student's *t*-test. A Bonferroni-corrected *t*-test was used to assess differentially abundant bacterial species between pro-inflammatory and pro-survival environments. Tests between multiple groups used one-way ANOVA with either Tukey's or Sidak's multiple comparisons. Tests between multiple groups over time used two-way ANOVA with Dunnett's multiple comparisons. Survival curves were evaluated by generalized Wilcoxon test.

Reporting summary

Further information on research design is available in the Nature Research Reporting Summary linked to this paper.

Data availability

The 16S rDNA sequencing dataset are available through the Gene Expression Omnibus repository at GSE147325. All other data generated or analysed are included in the published Article and its Supplementary Information.

38. DeSantis, T. Z. et al. Greengenes, a chimera-checked 16S rRNA gene database and workbench compatible with ARB. *Appl. Environ. Microbiol.* **72**, 5069–5072 (2006).
39. Caporaso, J. G. et al. QIIME allows analysis of high-throughput community sequencing data. *Nat. Methods* **7**, 335–336 (2010).
40. Henderson, K. S. et al. Efficacy of direct detection of pathogens in naturally infected mice by using a high-density PCR array. *J. Am. Assoc. Lab. Anim. Sci.* **52**, 763–772 (2013).

Acknowledgements Support to K.E. was provided by The Merkin Fund at the Broad Institute, Target ALS, NIH 5R01NS089742, Harvard Stem Cell Institute and UCB. A.B. was supported by NIH 5K99AG057808-02, M.F.W. was supported by NIH 1K99MH119327-01. We thank J. Wang for providing faeces from mice housed Johns Hopkins University.

Author contributions A.B., M.F.W., J.M. and K.E. conceived the study. Experiments were performed by A.B. (Figs. 1–4, Extended Data Figs. 1–9), F.L. (Fig 1, Extended Data Fig. 2), M.F.W. (Fig. 1, Extended Data Fig. 2), K.S.S. (Fig. 4, Extended Data Figs. 8, 9), A.C. (Figs. 2–4, Extended Data Figs. 3–9), J.M. (Figs. 1–3, Extended Data Figs. 2–6, 8), N.v.G. (Extended Data Fig. 2), J.-Y.W. (Fig. 4, Extended Data Fig. 8), J.K. and G.G. (Extended Data Fig. 8), and M.Q. and P.E. and C.C. (Figs. 2, 3, Extended Data Figs. 3, 4, 8). A.B., F.L., K.S.S., J.K., G.G, N.v.G., J.-Y.W., O.P., I.K., D.T.S. and K.E. interpreted results. A.B. and K.E. wrote the manuscript.

Competing interests K.E. is a co-founder of Q-State Biosciences, Quralis and Enclear Therapies.

Additional information
Supplementary information is available for this paper at https://doi.org/10.1038/s41586-020-2288-7.
Correspondence and requests for materials should be addressed to K.E.
Peer review information *Nature* thanks Michael Fischbach, Aaron D. Gitler and the other, anonymous, reviewer(s) for their contribution to the peer review of this work.
Reprints and permissions information is available at http://www.nature.com/reprints.